POLITECNICO DI TORINO
Repository ISTITUZIONALE

# Micromechanics of periodically heterogeneous materials using higher-order beam theories and the mechanics of structure genome

*Original*
Micromechanics of periodically heterogeneous materials using higher-order beam theories and the mechanics of structure genome / GARCIA DE MIGUEL, Alberto; Pagani, Alfonso; Yu, Wenbin; Carrera, Erasmo. - In: COMPOSITE STRUCTURES. - ISSN 0263-8223. - 180:(2017), pp. 484-496. [10.1016/j.compstruct.2017.08.025]

*Availability:*
This version is available at: 11583/2678643 since: 2017-08-29T16:36:44Z

*Publisher:*
Elsevier Ltd

*Published*
DOI:10.1016/j.compstruct.2017.08.025

*Terms of use:*

This article is made available under terms and conditions as specified in the corresponding bibliographic description in the repository

*Publisher copyright*

(Article begins on next page)

12 October 2024

# Micromechanics of periodically heterogeneous materials using higher-order beam theories and the mechanics of structure genome

A.G. de Miguel*[1], A. Pagani†[1], W. Yu‡[2], and E. Carrera§[1]

[1]MUL[2] Group, Department of Mechanical and Aerospace Engineering, Politecnico di Torino, Turin, Italy

[2]School of Aeronautics and Astronautics, Purdue University, West Lafayette, IN, United States

*Ph.D. Student, alberto.garcia@polito.it

†Assistant Professor, alfonso.pagani@polito.it

‡Professor of Aeronautics and Astronautics, wenbinyu@purdue.edu

§Professor of Aerospace Structures and Aeroelasticity, erasmo.carrera@polito.it

# *Abstract*

*A novel approach for the micromechanical analysis of periodically heterogeneous composite materials is proposed in this paper. It is based on the use of refined beam theories for the modeling of the microstructure and the mechanics of structure genome (MSG) for the derivation of the governing equations of the unit cell problem. On the one hand, MSG is recalled to decouple the multiscale problem into global and local analysis, providing the constitutive information and the local fields with no need of ad-hoc assumptions, nor multiple loading steps. On the other hand, the Carrera Unified Formulation (CUF) is employed to generate higher-order beam models that show the same accuracy as conventional solid elements with reduced computational efforts. Accordingly, the main direction of the constituents (e.g. the fibre direction) is discretized by means of one-dimensional finite elements whereas the cross-section is hierarchically enriched with a set of Legendre-based polynomials with non-local capabilities. In addition, the implementation of a non-isoparametric mapping technique permits the representation of the exact geometry of the constituents with no additional costs. The validity and efficiency of the proposed model is assessed through comparison with several benchmark solutions of fibre reinforced and particle reinforced composites.*



**Keywords**: Micromechanics, Refined beam theories, Carrera Unified Formulation, Mechanics of Structure Genome.

# 1 Introduction

Composite materials are nowadays employed in applications that require a good balance between mechanical properties and weight, such as aerospace, automotive, naval or wind energy structures. However, despite its successful introduction, see for instance the B787 Dreamliner or the Formula 1 cars, and the experiences learned during the past decades, the correct prediction of the strength and failure of these structures is still an unfinished target and there is a continuous need for novel simulation techniques. The main complexity of the problem resides in the different scales that play a role in the structural problem, which neglects the use of direct numerical simulation techniques due to the enormous computational costs it would required. A solution is found in the multiscale modeling, in which the problem is treated in several steps accounting for the different length scales. A bottom-up transfer of information is then performed to link all the analysis from the constituent level to the macroscopic working structure, as depicted in Llorca *et al.* [1]. In this framework, the *computational micromechanics* serve to solve the microstructural problem to provide accurate constitutive models and local responses that can be used for the structural analysis at the laminate level, see [2, 3].

Micromechanical modeling methods are useful tools to acquire information about how the microscopic details, such as the arrangement of the fibres, their volume fraction or the geometry of the constituents, affect the global response of the homogenized equivalent material. This research field is in constant evolution and several analytical, semi-analytical and numerical methods have been proposed in the last decades. Reviews of different homogenization approaches are included in [4, 5, 6]. Many of these methods are based on the assumption that the arrangement of reinforcements follows a regular, periodic pattern, and recall the concept of the *repeating unit cell* (hereinafter RUC), that is defined as the minimum geometrical entity that can be periodically repeated over the space to shape the higher scale structure. Some approaches make use of analytical formulations to solve the RUC problem, such as the various rules of mixtures [7], the Hashin-Shtrikman bounds [8], the Mori-Tanaka method [9], the generalized self-consistent method [10] or the elasticity-based cell method [11, 12]; whereas others provide approximate solutions that are suitable for more generic cases, such as the method of cells [13], the generalized method of cells [14] and the high-fidelity method of cells [15] or the mathematical homogenization theories [16, 17]. Another wide-spread technique is based on the application of appropiate boundary tractions or boundary displacements to a *representative volume element* (RVE) and then perform conventional stress analysis to obtain the elastic proeprties [18].

In the present work, the authors make use of the mechanics of structure genome (MSG), introduced by Yu [19], to solve the RUC problem by means of a novel 1D approach. This method is based on the concept of the *structure genome* (SG), that is defined as the smallest mathematical building block of the structure. The SG can be a line that accounts for the different plies in laminates, a surface that includes the different phases of materials showing 2D heterogeneities (e.g. fibre reinforced composites), or, in general cases, the 3D repeating

body for microstructures featuring variation of the phases over the three spatial coordinates. MSG exploits the variational asymptotic method (VAM) [20] to solve mechanical problems that involve smaller parameters and has been successfully applied to provide efficient solutions for composite problems, see [21, 22]. VAM can be used to carry out an asymptotic analysis of the RUC problem and obtain the effective properties and the local solutions of periodically heterogeneous materials [23] with great accuracy and efficiency.

Most of the aforementioned micromechanical theories involve a computational problem that has to be solved to produce the constitutive information. In composite simulation the size of this problem can be a major drawback if a detailed study is needed. The Carrera Unified Formulation (CUF) [24] was introduced as a tool to reduce general 3D structural problems to less demanding 1D [25, 26] or 2D [27, 28] models providing the same levels of accuracy. In this sense, the limitations of classical beam and plate/shell theories are overcome by employing an arbitrary refinement of the kinematics and expressing the governing equations in a hierarchical, unified and compact manner, see the book of Carrera *et al.* [29]. Exploiting these capabilities, the RUC body can be modeled using beam elements along the fibre direction (if any), and non-local expansions of the unknown variables over the remaining two directions, see [30]. The recently introduced Hierarchical Legendre Expansion (HLE) [31] is used here to generate hierarchical refined models of the RUC in which the geometry of the constituents is captured exactly through a higher-order mapping technique. The validity and accuracy of the refined beam modeling to solve the micromechanical problem posed by means of MSG is presented and demonstrated.

The paper is organized as follows: initially, some insights of the RUC analysis are introduced in Section 2, followed by a description of the variational asymptotic method for periodically heterogeneous materials in Section 3. The introduction of refined CUF beam models in micromechanical analysis can be found in Section 4, with a focus in the HLE modeling of the RUC problem and the subsequent 1D formulation. The numerical assessment is presented in Section 5, where results of fibre reinforced and particle inclusions are included. Finally, the conclusions are depicted in Section 6.

# 2 Premises: the unit cell problem

Let us consider a composite structure wherein the microstructure is periodically distributed over the volume. The RUC is defined as the smallest building block that contains all the information needed to identify the material properties. Figure 1 shows a typical periodically heterogeneous material and a zoom into the correspondent RUC. The macroscopic properties are defined in a global coordinate system, $\boldsymbol{x} = \{x_1, x_2, x_3\}$, whereas $\boldsymbol{y} = \{y_1, y_2, y_3\}$ defines the local reference system of the RUC. Micromechanical analyses serve to two purposes:

- Obtain effective properties of heterogeneous material represented by the RUC, to be used as inputs for the equivalent homogeneous material employed in the higher scale

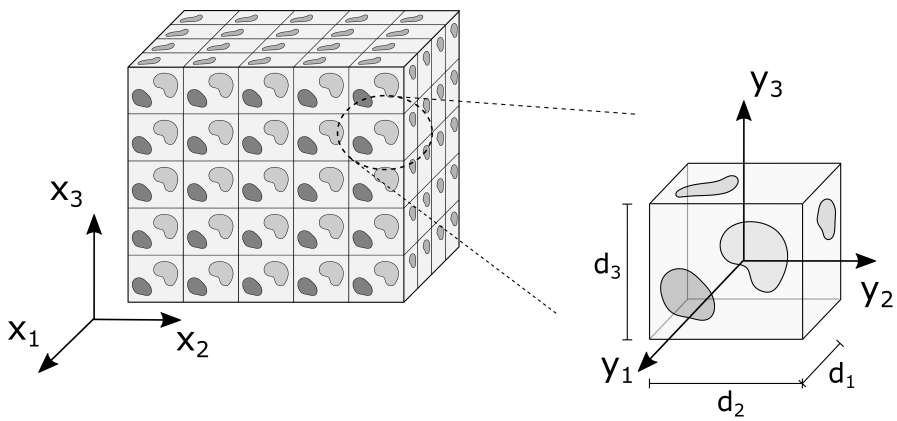


Figure 1: Coordinate reference systems of a periodic heterogeneous material and its RUC.

analysis.

- Recover the displacements, strains and stresses local fields over the RUC volume from the outputs of the macroscopic structural analysis at the points of interest.

The starting point of micromechanical analysis is the assumption that the RUC is much smaller than the global structure, such that $y_i = x_i/\delta$, where $\delta$ is a small scaling parameter that characterizes the dimension of the RUC. In essence, in micromechanics, the material properties obtained from the RUC analysis at the micro-scale are independent of the structural problem at the macro-scale, i.e. geometry, boundary conditions and loadings. In other words, they are considered as intrinsic properties of the material for the structural analysis. In addition, the local solutions have an average value over the RUC volume, which is equal to the global solution of the macroscopic problem. For instance, considering the displacement field, one can write

$$\frac{1}{V}\int_V u_i(\boldsymbol{x},\boldsymbol{y})\,dV = \bar{u}_i(\boldsymbol{x}) \tag{1}$$

where $V$ is the total volume of the cell. $u_i$ are the local displacements that depend both on the global and the local coordinates, $\boldsymbol{x}$ and $\boldsymbol{y}$ respectively, and $\bar{u}_i$ are the averaged displacements which only depend on the global reference system. In general, periodic boundary conditions are applied to ensure the compatibility of the deformations with respect to the neighboring RUCs. For a cell placed at a certain point of the structure, the periodicity can be expressed as:

$$\begin{aligned}
u_i(x_1,x_2,x_3;\frac{d_1}{2},y_2,y_3) &= u_i(x_1+d_1,x_2,x_3;-\frac{d_1}{2},y_2,y_3)\\
u_i(x_1,x_2,x_3;y_1,\frac{d_2}{2},y_3) &= u_i(x_1,x_2+d_2,x_3;y_1,-\frac{d_2}{2},y_3)\\
u_i(x_1,x_2,x_3;y_1,y_2,\frac{d_3}{2}) &= u_i(x_1,x_2,x_3+d_3;y_1,y_2,-\frac{d_3}{2})
\end{aligned} \tag{2}$$

# 3 Variational Asymptotic Method for RUCs

MSG is based on VAM, introduced by Berdichevskly [20], to provide efficient solutions for structural problems. VAM is a powerful tool for the study of stationary value problems in which certain terms can be identified as smaller than others. In problems governed by variational statements, VAM can be used to find the stationary points of a functional by performing an asymptotic expansion in terms of one or more small parameters. This can be very useful in mechanics, where many typical problems include one or several dimensions that are relatively small. For instance, in beam-like structures, the cross-section is usually considered smaller than the length according to a certain slenderness ratio, and in plate/shell problems the thickness of the wall is often negligible in comparison to the in-plane coordinates. In composite materials, VAM can be considered a natural approach for the multiscale analysis, given the several geometrical scales that play a role in the structural problem.

It is clear that for the problem posed in Figure 1 the smallest building block is equivalent to the RUC. In MSG, the solution of the stationary value problem is provided by minimizing the difference between the strain energies of the heterogeneous structure and the equivalent homogeneous material, represented by the following functional:

$$\Pi = \left\langle \frac{1}{2}\, C_{ijkl}\, \varepsilon_{ij}\, \varepsilon_{kl} \right\rangle - \frac{1}{2}\, C^{*}_{ijkl}\, \bar{\varepsilon}_{ij}\, \bar{\varepsilon}_{kl} \tag{3}$$

where $\langle \bullet \rangle$ denotes the volume average $\frac{1}{V}\int_V \bullet\, dV$. The first term of the functional $\Pi$ corresponds to the strain energy of the heterogeneous body represented by the RUC, whereas the second is that of the homogeneous material. $C_{ijkl}$ is the fourth-order elastic tensor and $\varepsilon_{ij}$ is the second-order strain tensors. On other hand, $C^{*}_{ijkl}$ and $\bar{\varepsilon}_{ij}$ refer to the global solutions.

As it is usual in micromechanics, the local displacements, $u_i$, can be written as the sum of the global displacements, $\bar{u}_i$, plus the difference between both, as follows

$$u_i(\boldsymbol{x};\boldsymbol{y}) = \bar{u}_i(\boldsymbol{x}) + \delta\, \chi_i(\boldsymbol{x};\boldsymbol{y}) \tag{4}$$

where $\chi_i$ are denoted as fluctuation functions, which are scaled down using $\delta$.

Due to the different coordinate reference systems involved in the multiscale problem, the derivative of a field of the type $f(\boldsymbol{x};\boldsymbol{y})$ acquires the following form

$$\frac{\partial f}{\partial x_j} + \frac{1}{\delta}\frac{\partial f}{\partial y_j} \tag{5}$$

Therefore, applying Eq. (5) to the derivatives of Eq. (4), and discarding smaller terms according to the VAM [20], the strain variables can be written as

$$\varepsilon_{ij}(\boldsymbol{x};\boldsymbol{y}) = \bar{\varepsilon}_{ij}(\boldsymbol{x}) + \chi_{(i,j)}(\boldsymbol{x};\boldsymbol{y}) \tag{6}$$

where

$$\bar{\varepsilon}_{ij}(\boldsymbol{x}) = \frac{1}{2}\Big(\frac{\partial \bar{u}_i(\boldsymbol{x})}{\partial x_j} + \frac{\partial \bar{u}_j(\boldsymbol{x})}{\partial x_i}\Big) \tag{7}$$

and

$$\chi_{(i,j)}(\boldsymbol{x};\boldsymbol{y}) = \frac{1}{2}\Big(\frac{\partial \chi_i(\boldsymbol{x};\boldsymbol{y})}{\partial y_j} + \frac{\partial \chi_j(\boldsymbol{x};\boldsymbol{y})}{\partial y_i}\Big) \tag{8}$$

According to Eq. (1), one can write

$$\bar{u}_i = \langle u_i \rangle \qquad\qquad \bar{\varepsilon}_{ij} = \langle \varepsilon \rangle \tag{9}$$

which implies the following constrains to the fluctuation unknowns

$$\langle \chi_i \rangle = 0 \qquad\qquad \langle \chi_{(i,j)} \rangle = 0 \tag{10}$$

Now, making use of the displacement and strain definitions of Eq. (4) and Eq. (6), respectively, and considering the second term of Eq. (3) as invariable, the fluctuation unknowns, $\chi_i$, can be solved by minimizing the following functional

$$\Pi_1 = \frac{1}{2}\Big\langle C_{ijkl}\left(\bar{\varepsilon}_{ij} + \chi_{(i,j)}\right)\left(\bar{\varepsilon}_{kl} + \chi_{(k,l)}\right)\Big\rangle \tag{11}$$

subjected to the constrains of Eq. (10).

In previous works of MSG for the RUC homogenization, the problem is formulated conveniently to be solved by conventional finite element analysis (FEA) techniques, implemented in a general-purpose multiscale constitutive modeling code called SwiftComp$^{TM}$ [32]. The novelty of the present paper arises herein, where the authors propose an efficient manner to solve the computational problem based on the use of refined beam models.

# 4 Refined beam models for the RUC problem

Although closed-form solutions are very useful in micromechanics, they are only available in a few simple problems. In order to deal with more complex cases, it is necessary to make use of numerical analysis to obtain approximate solutions. Depending on the geometrical features of the heterogeneous microstructure, MSG can be applied to solve a 2D problem for cases in which the phases vary only within a plane, such as fibre reinforced composites, or a 3D problem for multi-phase materials varying over the three directions, for instance in particle inclusions or woven-fibre composites. In this work, the governing equations of the 3D cells, previously obtained from MSG, are solved by means of a 1D unified formulation.

Consider a local coordinate system for the micro-scale problem as the one shown in Figure 2. For illustrative purposes, a fibre reinforced microstructure featuring a typical square pack is accounted for, although more general cases can be analysed with this approach, as it will be shown later. The beam axis, $y_1$, is chosen to be the fibre direction, whose total length is equal to $L$, whereas the heterogeneities represented by the fibre-matrix phases lie on the $y_2y_3$-plane,

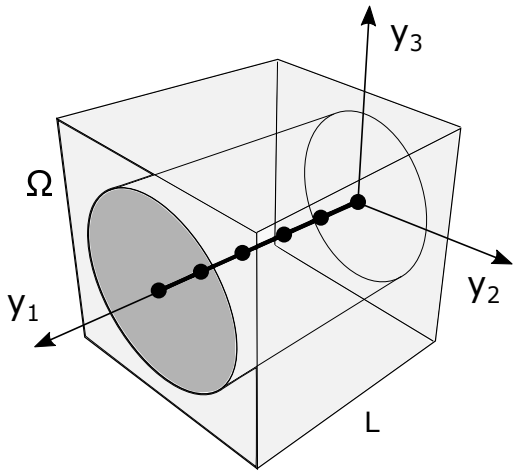


Figure 2: Reference system for the beam modeling of the RUC.

in correspondence with the cross-section of the beam, $\Omega$. It is obvious that classical beam models are not a suitable choice to solve the RUC problem. Classical models, for instance those based on the Timoshenko assumptions [33], are only valid for high slenderness ratios and produce a cross-section that remains plane and rigid due to the kinematic assumptions. These characteristics prevent its use in problems as the one shown in Figure 2, where different materials coexist, the body is short and high gradients are present in the displacement, strain and stress fields.

To overcome this issues, the CUF sets a framework in beam modeling in which the kinematic assumptions are axiomatically introduced in the structural analysis. In this manner, higher-order effects, such as warping, in-plane deformations or component-wise solution fields, can be captured by conveniently selecting the theory of structure. For the RUC problem, the fluctuation unknowns can be expanded over the cross-section by means of arbitrary functions of the $y_2$ and $y_3$ coordinates, as follows

$$\boldsymbol{\chi}(\boldsymbol{x}; y_1, y_2, y_3) = F_\tau(y_2, y_3)\, \boldsymbol{\chi}_\tau(\boldsymbol{x}; y_1) \quad \tau = 1, 2, ..., M \tag{12}$$

where $\boldsymbol{\chi}$ is the vector of the fluctuations, $F_\tau$ are the expanding functions and $\boldsymbol{\chi}_\tau$ is the vector of the generalized fluctuations of the beam along the fibre-direction. The repeated subscript $\tau$ denotes summation and $M$ is the total number of expansion terms assumed for the kinematic field. The choice of $F_\tau$ defines the beam theory of the analysis. This feature makes CUF a powerful tool for the development and assessment of structural models. In the past years, Taylor [25, 34], Chevishev [35], zig-zag [36] and Lagrange [26] theories were employed to generate advanced beam models for many applications.

For the accurate micromechanical analysis of heterogeneous composites, some specific characteristics are required from the beam theory. It should account independently for the kinematics of each component (fibre, particle, matrix, ...) to capture the inherent discontinuities at the interfaces and, in addition, a non-local distribution of the degrees of freedom over the cross-section is highly convenient for the application of the boundary conditions of Eq.

(11). With these characteristics in mind, a recently developed model based on hierarchical higher-order polynomials, called Hierarchical Legendre Expansions, is chosen in this paper to carry out the micromechanical analysis.

## 4.1 Hierarchical Legendre Expansions (HLE)

HLE beam models, introduced by Carrera *et al.* [31], exploit the hierarchical characteristics of Legendre-based polynomials to construct a set of high-order polynomials that are used as arbitray functions over the cross-section, $F_\tau$. It is inspired in the original arrangement of shape functions proposed by Szabó and Babuška [37] for the development of the p-version of the FEM. In HLE, the expansion functions are defined in a natural plane and then mapped into the cross-section, enabling a straightfordward construction of Layer-Wise [38] and Component-Wise [39] models. Figure 3 shows the set of $F_\tau$ expanding functions that are employed to generate first to seventh order models. One can note that the displacement field, and therefore the accuracy, is enriched by adding polynomials of higher-order.

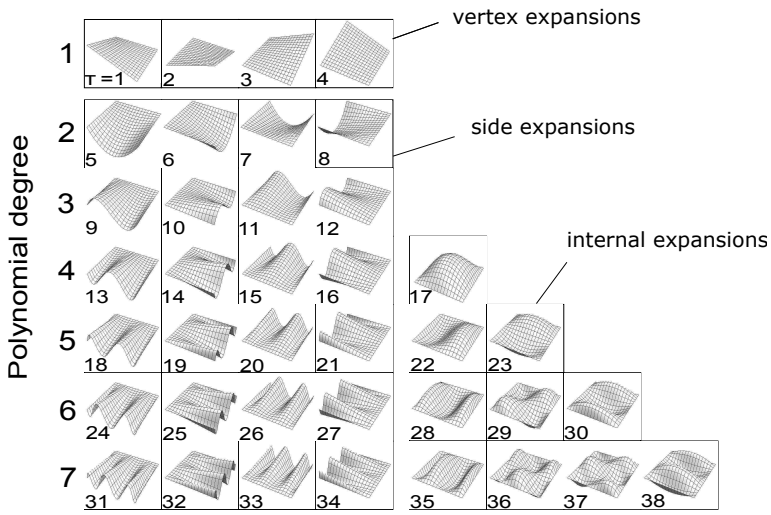


Figure 3: Set of Legendre functions employed over the cross-section.

There are three types of expansion functions: vertex, side and internal. The vertex functions correspond to the first order model and are defined as:

$$F_\tau = \frac{1}{4}(1 - r_\tau r)(1 - s_\tau s) \qquad \tau = 1, 2, 3, 4 \tag{13}$$

where $r$ and $s$ vary over the natural frame between $-1$ and $+1$, and $r_\tau$ and $s_\tau$ represent the vertex coordinates of the quadrilateral domain. For higher-order models, an increasing

number of side functions are added to the displacement field. These can be written as follows

$$F_\tau(r,s) = \frac{1}{2}(1-s)\phi_{p_b}(r) \qquad \tau = 5, 9, 13, 18, ... \tag{14}$$

$$F_\tau(r,s) = \frac{1}{2}(1+r)\phi_{p_b}(s) \qquad \tau = 6, 10, 14, 19, ... \tag{15}$$

$$F_\tau(r,s) = \frac{1}{2}(1+s)\phi_{p_b}(r) \qquad \tau = 7, 11, 15, 20, ... \tag{16}$$

$$F_\tau(r,s) = \frac{1}{2}(1-r)\phi_{p_b}(s) \qquad \tau = 8, 14, 16, 21, ... \tag{17}$$

where $\phi_p$ corresponds to the one-dimensional internal Legendre-type modes, as described in [37]. They are defined for $p \geq 2$, where $p$ is the polynomial order of the beam theory. For models of $p \geq 4$ order, $(p-2)(p-3)/2$ internal functions are also included in the kinematics. These functions vanish over the edges of the domain and have the following form:

$$F_{28}(r,s) = \phi_4(r)\phi_2(s) \tag{18}$$

$$F_{29}(r,s) = \phi_3(r)\phi_3(s) \tag{19}$$

$$F_{30}(r,s) = \phi_2(r)\phi_4(s) \tag{20}$$

In HLE beam modeling, the cross-section can be divided in several expansion domains, enabling the representation of generic geometries of the microstructure. In addition, the different constituents within the RUC can be independently modeled, imposing the compatibility of the displacements at the interfaces of the domains. The periodic boundary conditions over the $y_2y_3$-plane can be easily modeled as

$$\boldsymbol{\chi}_\tau^+ = \boldsymbol{\chi}_\tau^- \tag{21}$$

where the superscripts $+$ and $-$ refer to the opposite sides of the cross-section surface. It is worthy to note that Eq. (21) involves the vertex and edge fluctuation variables placed in the boundaries of the cross-section.

Due to the high polynomial orders that can be used in HLE theories, it is convenient to keep the domains as large as possible. To fulfill these premise, a non-isoparametric mapping technique is applied to adapt the edges of the HLE domains to the geometrical features of the different components of the microstructure. Any geometrical description can be in this manner parametrized and introduced into the model through the use of blending functions, as proposed by Gordon and Hall [40]. This method was first employed in HLE modeling by Pagani *et al.* [41] to curve the section of thin-walled beams and it is applied here to describe the exact geometry of the fibres embedded in the RUC, as shown in Figure 4.

Using the blending function method, the exact geometry of an arbitrary component in the

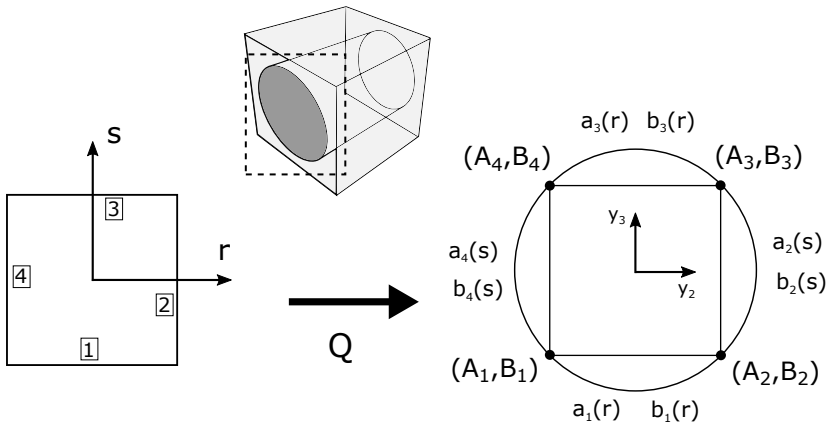


Figure 4: Mapping of the fibre section of the RUC through the blending function method.

$y_2y_3$-plane is directly introduced into the mapping functions, $\mathbf{Q}$, as follows:

$$\begin{aligned} y_2 = Q_a(r,s) =& \frac{1}{2}(1-s)a_1(r) + \frac{1}{2}(1+r)a_2(s) + \frac{1}{2}(1+s)a_3(r) \\ &+ \frac{1}{2}(1-r)a_4(s) - F_\tau(r,s)\, r_\tau \\ y_3 = Q_b(r,s) =& \frac{1}{2}(1-s)b_1(r) + \frac{1}{2}(1+r)b_2(s) + \frac{1}{2}(1+s)b_3(r) \\ &+ \frac{1}{2}(1-r)b_4(s) - F_\tau(r,s)\, s_\tau \end{aligned} \tag{22}$$

where $\tau = 1, ..., 4$ and $a_\tau$ and $b_\tau$ are the parametric curves of the edges. This approach sets a new framework for the numerical analysis of microstructures, in which the geometry of the model is fixed at the beginning and the accuracy of the micromechanical analysis can be tuned through the polynomial order of the theory of structure. In a few words, the exact geometry of the fibre can be modeled by one single expansion and there is no need of further re-meshing procedures to assess the convergence of the analysis.

## 4.2 Finite element approximation

Many different approaches are available to solve the numerical problem along the beam axis, $y_1$. Among these, the finite element method (FEM) is probably the most extended one. In the present work, the fibre direction is discretized by means of standard beam elements. Accordingly, the generalized fluctuation unknowns, $\boldsymbol{\chi}_\tau$, are interpolated with Lagrange shape functions of the $y_1$ coordinate

$$\boldsymbol{\chi}_\tau(\boldsymbol{x}; y_1) = N_i(y_1)\, \boldsymbol{\chi}_{\tau i}(\boldsymbol{x}) \quad i = 1, 2, ..., n \tag{23}$$

where $\boldsymbol{\chi}_{\tau i}(\boldsymbol{x})$ is the nodal unknown vector and $n$ is the total number of beam nodes.

Rearranging the global strains in vectorial form,

$$\bar{\boldsymbol{\varepsilon}}^T = \left\{ \begin{array}{cccccc} \bar{\varepsilon}_{11} & \bar{\varepsilon}_{22} & \bar{\varepsilon}_{33} & 2\,\bar{\varepsilon}_{23} & 2\,\bar{\varepsilon}_{13} & 2\,\bar{\varepsilon}_{12} \end{array} \right\} \tag{24}$$

it is possible to write the geometrical relations as

$$\boldsymbol{\varepsilon} = \bar{\boldsymbol{\varepsilon}} + \mathbf{D}\,\boldsymbol{\chi} \tag{25}$$

where $\mathbf{D}$ is the differential operator defined as follows:

$$\mathbf{D} = \begin{bmatrix} \partial_{y_1} & 0 & 0 \\ 0 & \partial_{y_2} & 0 \\ 0 & 0 & \partial_{y_3} \\ 0 & \partial_{y_3} & \partial_{y_2} \\ \partial_{y_3} & 0 & \partial_{y_1} \\ \partial_{y_2} & \partial_{y_1} & 0 \end{bmatrix} \tag{26}$$

with $\partial_{y_i} = \partial(\bullet)/\partial y_i$ and $i = 1, 2, 3$.

In order to solve numerically the micromechanical problem, the functional of Eq. (11) can be rewritten as

$$\Pi_1^* = \frac{1}{2} \int_V (\bar{\boldsymbol{\varepsilon}} + \mathbf{D}\,\boldsymbol{\chi})^T \boldsymbol{C}\,(\bar{\boldsymbol{\varepsilon}} + \mathbf{D}\,\boldsymbol{\chi})\; dV \tag{27}$$

which is subjected to the periodic boundary constrains of Eq. (21) for the boundaries of the RUC laying on the sides of the cross-section, i.e. parallel to the fibre direction, and

$$\boldsymbol{\chi}_{\tau 1} = \boldsymbol{\chi}_{\tau n} \tag{28}$$

for the boundary sections orthogonal to the fibre, where 1 and $n$ are the first and last beam nodes. As outlined in [23], the volume constrains, represented by the second term of Eq. (11), do not influence the variation of $\Pi_1^*$, although they are useful to obtain a unique solution for $\boldsymbol{\chi}_{\tau i}$. Substituting Eq. (23) into Eq. (12), and the latter into Eq. (27), the CUF form of the functional $\Pi_1^*$ reads

$$\Pi_1^* = \frac{1}{2}\left(\boldsymbol{\chi}_{sj}^T\, \boldsymbol{E}^{\tau sij}\, \boldsymbol{\chi}_{\tau i} + 2\,\boldsymbol{\chi}_{sj}^T\, \boldsymbol{D}_{h\varepsilon}^{sj}\, \bar{\boldsymbol{\varepsilon}} + \bar{\boldsymbol{\varepsilon}}^T\, \boldsymbol{D}_{\varepsilon\varepsilon}\, \bar{\boldsymbol{\varepsilon}}\right) \tag{29}$$

where

$$\begin{aligned} \boldsymbol{E}^{\tau sij} &= \int_\Omega \int_l (\boldsymbol{D}(F_\tau N_i \boldsymbol{I}))^T\, \boldsymbol{C}\, \boldsymbol{D}(F_s N_j \boldsymbol{I})\, d\Omega\, dy_1 \\ \boldsymbol{D}_{h\varepsilon}^{\tau i} &= \int_\Omega \int_l (\boldsymbol{D}(F_\tau N_i \boldsymbol{I}))^T\, \boldsymbol{C}\, d\Omega\, dy_1 \\ \boldsymbol{D}_{\varepsilon\varepsilon} &= \int_\Omega \int_l \boldsymbol{C}\, d\Omega\, dy_1 \end{aligned} \tag{30}$$

being $\boldsymbol{I}$ the $3 \times 3$ identity matrix. $\boldsymbol{E}^{\tau sij}$ and $\boldsymbol{D}_{h\varepsilon}^{\tau i}$ are the fundamental nucleus of the RUC problem, that contain all the basic information for the numerical model based on MSG. On the other hand, $\boldsymbol{D}_{\varepsilon\varepsilon}$ is the effective stiffness matrix of the material by volume average. Following the matrix operations, one can easily obtain that $\boldsymbol{E}^{\tau sij}$ is a $3 \times 3$ matrix, whereas $\boldsymbol{D}_{h\varepsilon}^{\tau i}$ is a $3 \times 6$ matrix and $\boldsymbol{D}_{\varepsilon\varepsilon}$ is a $6 \times 6$ matrix. The $\tau$ and $s$ subscripts refer to the loop over the

cross-sectional expansions, whereas the $i$ and $j$ subscripts refer to the beam nodes. Any order theory and beam discretization can be automatically generated by appropriately expanding the fundamental nuclei along $\tau$, $s$, $i$ and $j$, see the book of Carrera *et al.* [29]. For the sake of completeness, the explicit expressions of $\boldsymbol{E}^{\tau sij}$ and $\boldsymbol{D}_{h\varepsilon}^{\tau i}$ are provided in Apendix A for orthotropic materials.

Performing the variation of $\Pi_1^*$, one finds that the solution which minimizes the functional is provided by the following expression

$$\boldsymbol{E}^{\tau sij}\,\boldsymbol{\chi}_{\tau i} = -\boldsymbol{D}_{h\varepsilon}^{sj}\,\bar{\boldsymbol{\varepsilon}} \tag{31}$$

According to the linearity of the system of equations in Eq. (31), $\boldsymbol{\chi}_{\tau i}$ is a linear function of $\bar{\boldsymbol{\varepsilon}}$, therefore it can be written as

$$\boldsymbol{\chi}_{\tau i}(\boldsymbol{x}) = \boldsymbol{\chi}_{\tau i0}\,\bar{\boldsymbol{\varepsilon}}(\boldsymbol{x}) \tag{32}$$

As a result, the system of the computational problem becomes:

$$\boldsymbol{E}^{\tau sij}\,\boldsymbol{\chi}_{\tau i0} = -\boldsymbol{D}_{h\varepsilon}^{sj} \tag{33}$$

where $\boldsymbol{\chi}_{\tau i0}$ is a $3 \times 6$ array containing the fluctuation solutions.

Once the linear system of Eq. (33) is solved, the effective properties of the heterogeneous material can be straightforwardly computed. Inherently, it is considered that the energy stored in the equivalent homogenized material is equal to that of the original heterogeneous material. Substituting Eq. (31) into the strain energy of Eq. (29), and making the energetic equivalence, the effective stiffness matrix, $C^*$, reads:

$$\boldsymbol{C}^* = \frac{1}{V}\left(\boldsymbol{\chi}_{sj0}^T\,\boldsymbol{D}_{h\varepsilon}^{sj} + \boldsymbol{D}_{\varepsilon\varepsilon}\right) \tag{34}$$

where $C^*$ contains the material properties of the equivalent homogenized body.

If the local fields over the cell are needed, they can be directly recovered by simply introducing back the fluctuation solutions of Eq. (33) into the geometrical and constitutive definitions. Accordingly, the local strains are

$$\boldsymbol{\varepsilon} = \bar{\boldsymbol{\varepsilon}} + \boldsymbol{D}(F_\tau N_i\,\boldsymbol{\chi}_{\tau i0}\,\bar{\boldsymbol{\varepsilon}}) \tag{35}$$

and, then, the local stresses are directly computed from the Hooke's law of the original heterogeneous material

$$\boldsymbol{\sigma} = \boldsymbol{C}\,\boldsymbol{\varepsilon} \tag{36}$$

In the framework of MSG for the RUC problem, the fluctuation functions are obtained from the solution of the stationary value of the energy functional and no external loads are required to compute the effective properties of the homogenized material. In addition, due to the separation between the problem unknowns, $\boldsymbol{\chi}_{\tau i0}$, and the global strains, $\bar{\boldsymbol{\varepsilon}}$, the local fields can be computed for arbitrary inputs with only a single run of the code. Refined beam models

are clearly convenient in terms of computational efforts when dealing with microstructures that feature predominating directions in the phases, such us fibre reinforced composites, although its use can be extended to other typical 3D RUCs, such as particle inclusions, as it is shown in the following.

# 5 Numerical examples

The numerical examples included in the following are selected to validate the proposed approach and to show the capabilities of HLE beam models for the accurate RUC analysis. First, several well-known benchmark cases of unidirectional fibre reinforced and particle reinforced composites are solved and the effective stiffness properties are presented and compared to those from the literature. Then, the effectiveness of the 1D formulation and the MSG for the homogenization and recovering problem is illustrated through direct comparison against already established micromechanical theories.

## 5.1 Fibre reinforced composites

### 5.1.1 Circular fibres

The first two cases deal with circular fibres embedded in a square pack: the boron-aluminum and the graphite-epoxy RUCs. These examples have been extensively studied in the literature and it is a usual test for new micromechanical formulations. Due to the arrangement of the constituents in this microstructure, the properties along the fibre-direction do not vary. This feature can be exploited to reduce the dimension of the cell while still obtaining the full set of effective properties. In this sense, the MSG-based code SwiftComp computes the same results for a fibre reinforced composite using a 2D and a 3D SG, see [19]. In beam modeling, this characteristic of the material can be conveniently handled to generate a reduced numerical model. It is clear that, given the arrangement of the phases in these RUCs, the fluctuation unknowns (and therefore, the strain and stress local fields) will be constant along the fibre direction. In such case, a single linear beam element is enough to interpolate the unknowns along the beam axis. In addition, according to Eq. (28) the first and last sections can be linked using a master-slave technique, leaving only a single effective section to be analysed.

For the boron-aluminum microstructure, both fibre and matrix are considered isotropic: $E = 379.3$ GPa and $\nu = 0.1$ for the boron fibre, and $E = 68.3$ GPa and $\nu = 0.3$ for the aluminum matrix. The volume fraction of the fibre is equal to 0.47. The distribution of HLE expansion domains over the section of the RUC is illustrated in Figure 5 (a). One domain models the fibre, whereas the matrix is represented by four domains, for connectivity reasons. At each of these domains, the polynomial order of the expansion can be set arbitrarily by the user. Table 1 shows the effective properties of the equivalent transversely isotropic material for increasing polynomial orders of the beam model. The number of the model name denotes the order of the theory (for instance, HL2 is the second order beam model). Several already

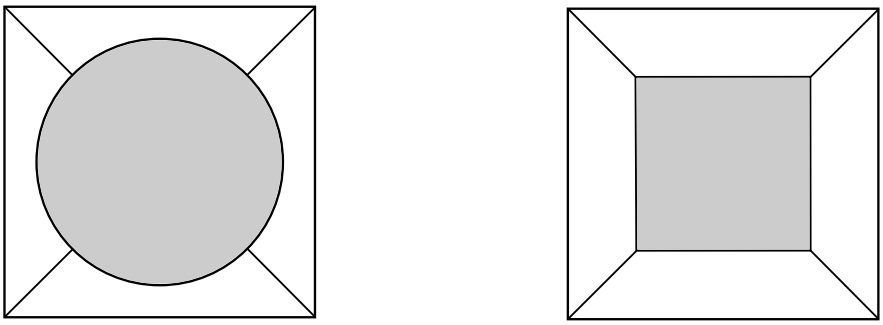

(a) Circular fibre (b) Square fibre

Figure 5: Distribution of expansion domains over the cross-section for fibre-reinforced composites.

established micromechanical solutions are also included for comparison reasons, including FEM-based RVE analysis by Sun and Vaidya [18], method of cells (MOC) by Aboudi [13], generalized method of cells (GMC) by Paley and Aboudi [14], high-fidelity generalized method of cells (HFGMC) by Aboudi *et al.* [15], elasticity-based cell method (ECM) by Williams [11] and SwiftComp [32].

| Model | $E_1$ [GPa] | $E_2$ [GPa] | $G_{12}$ [GPa] | $G_{23}$ [GPa] | $\nu_{12}$ | $\nu_{23}$ |
|---|---|---|---|---|---|---|
| | | | Literature | | | |
| FEM [18] | 215 | 144 | 57.2 | 45.9 | 0.19 | 0.29 |
| MOC [13] | 215 | 142.6 | 51.3 | 43.7 | 0.20 | 0.25 |
| GMC [14] | 215.0 | 141.0 | 51.20 | 43.70 | 0.197 | 0.261 |
| HFGMC [15] | 215.4 | 144.0 | 54.34 | 45.83 | 0.195 | 0.255 |
| ECM [11] | 215 | 143.4 | 54.3 | 45.1 | 0.19 | 0.26 |
| SwiftComp [32] | 215.3 | 144.1 | 54.39 | 45.92 | 0.195 | 0.255 |
| | | | CUF-MSG | | | |
| HL2 | 215.65 | 145.99 | 55.16 | 47.65 | 0.193 | 0.250 |
| HL3 | 215.57 | 144.96 | 54.53 | 46.55 | 0.194 | 0.251 |
| HL4 | 215.57 | 144.32 | 54.44 | 45.99 | 0.194 | 0.254 |
| HL5 | 215.56 | 144.14 | 54.42 | 45.86 | 0.194 | 0.254 |
| HL6 | 215.56 | 144.11 | 54.42 | 45.84 | 0.194 | 0.255 |
| HL7 | 215.56 | 144.10 | 54.42 | 45.84 | 0.194 | 0.255 |
| HL8 | 215.56 | 144.10 | 54.42 | 45.84 | 0.194 | 0.255 |

Table 1: Effective properties of the boron-aluminum cell.

For the second assessment, the fibre is made of a transverse isotropic AS4 graphite material with $E_1 = 235$ GPa, $E_2 = 14$ GPa, $G_{12} = 28$ GPa, $G_{23} = 5.6$ GPa, $\nu_{12} = 0.2$ and $\nu_{23} = 0.25$. The matrix is isotropic (3501-6 epoxy) with $E = 4.8$ GPa and $\nu = 0.34$. The fibre is also circular and the fibre volume fraction is equal to 0.60. As for the previous example, different polynomial orders are shown in Table 2, together with the solutions from the literature. In view of the results obtained for these cases, it should be highlighted that:

- The solutions obtained with HLE beam models are in good agreement with those of the

literature. Both the longitudinal and the transverse effective properties are computed with less than 1 % of difference in comparison to those of SwiftComp.

- The convergence of the proposed model is extremely fast, showing that the polynomial orders can be low for the computation of the effective properties. On the other hand, the computational costs are in all cases fairly reduced. For instance, the HL2 model employs 120 degrees of freedom, whereas the HL8 model goes up to 957.

| Model | $E_1$ [GPa] | $E_2$ [GPa] | $G_{12}$ [GPa] | $G_{23}$ [GPa] | $\nu_{12}$ | $\nu_{23}$ |
|---|---|---|---|---|---|---|
| | | | Literature | | | |
| FEM [18] | 142.6 | 9.60 | 6.00 | 3.10 | 0.25 | 0.35 |
| MOC [13] | 143 | 9.6 | 5.47 | 3.08 | 0.25 | 0.35 |
| GMC [14] | 143.0 | 9.47 | 5.68 | 3.03 | 0.253 | 0.358 |
| HFGMC [15] | 142.9 | 9.61 | 6.09 | 3.10 | 0.252 | 0.350 |
| ECM [11] | 143 | 9.6 | 5.85 | 3.07 | 0.25 | 0.35 |
| SwiftComp [32] | 142.9 | 9.61 | 6.10 | 3.12 | 0.252 | 0.350 |
| | | | CUF-MSG | | | |
| HL2 | 143.17 | 9.70 | 6.29 | 3.19 | 0.252 | 0.346 |
| HL4 | 143.16 | 9.64 | 6.09 | 3.12 | 0.252 | 0.349 |
| HL6 | 143.16 | 9.62 | 6.09 | 3.12 | 0.252 | 0.350 |
| HL8 | 143.16 | 9.62 | 6.08 | 3.12 | 0.252 | 0.350 |

Table 2: Effective properties of the graphite-epoxy cell.

### 5.1.2 Square fibre

The next two examples consider a square inclusion embedded in a matrix. These are a tungsten-copper composite and a tungsten-void cell. Both metals are considered isotropic: $E = 395$ GPa and $\nu = 0.28$ for the tungsten inclusion, and $E = 127$ GPa and $\nu = 0.34$ for the copper matrix. The distribution of domains over the cross-sectional surface is equivalent to that of the previous cases, although now no mapping technique is required since all the interfaces are straight, see Figure 5 (b). Table 3 shows the effective transverse Young's modulus, $E_2$, of the tungsten-copper cell for different fibre volume fractions: 0.0204, 0.1837, 0.5102 and 0.7511, whereas Table 4 shows also $E_2$ for the void inclusion. The beam solutions are compared with those of MOC, ECM and Green's Function approach (G-F) from Williams [11], FEM-RVE from Yu and Tang [23] and SwiftComp. One can notice that, as for the previous cases, the results tend to converge to those of the references when increasing the order of the beam theory for all volume fractions considered.

## 5.2 Particle reinforced composites

When dealing with particles embedded in a matrix, the constituents vary over the three spatial directions. In such cases, 3D cells are always required and the computational costs heavily rise

| Model | 0.0204 | 0.1837 | 0.5102 | 0.7511 |
|---|---|---|---|---|
| | Literature | | | |
| FEM [23] | 129.92 | 156.51 | 229.71 | 301.0 |
| G-F [11] | 129.87 | 156.18 | 229.09 | 300.70 |
| MOC [11] | 129.50 | 154.40 | 226.20 | 299.00 |
| ECM($3^{rd}$ order) [11] | 129.50 | 154.60 | 226.60 | 299.10 |
| ECM($5^{rd}$ order) [11] | 129.80 | 156.50 | 229.50 | 300.80 |
| SwiftComp [32] | 129.92 | 156.51 | 229.72 | 300.99 |
| | CUF-MSG | | | |
| HL4 | 128.92 | 157.10 | 230.38 | 301.58 |
| HL6 | 128.77 | 156.78 | 230.11 | 301.35 |
| HL8 | 129.94 | 156.64 | 229.88 | 301.18 |

Table 3: Effective transverse Young's modulus, $E_2$ [GPa], of the tungsten-copper composite for various volume fractions.

| Model | 0.0204 | 0.1837 | 0.5102 | 0.7511 |
|---|---|---|---|---|
| | Literature | | | |
| FEM [23] | 120.22 | 81.70 | 39.75 | 18.25 |
| G-F [11] | 120.63 | 81.50 | 40.48 | 18.40 |
| MOC [11] | 110.20 | 75.27 | 38.22 | 17.99 |
| ECM($3^{rd}$ order) [11] | 110.20 | 75.38 | 38.23 | 17.99 |
| ECM($5^{rd}$ order) [11] | 118.90 | 80.97 | 39.64 | 18.20 |
| SwiftComp [32] | 120.22 | 81.73 | 39.75 | 18.25 |
| | CUF-MSG | | | |
| HL4 | 121.09 | 84.33 | 41.02 | 18.78 |
| HL6 | 120.70 | 82.87 | 40.41 | 18.51 |
| HL8 | 120.45 | 82.34 | 40.07 | 18.28 |

Table 4: Effective transverse Young's modulus, $E_2$ [GPa], of the void-copper composite for various volume fractions.

if one wants to accurately capture in detail the geometrical features. In this example, the 3D capabilities of the HLE beam models for the analysis of particle inclusions are presented. In order to account for the different constituents along the beam axis, a number of 1D elements are placed along the $y_1$ coordinate and the material properties of the related cross-sections are conveniently assigned, as shown in Figure 6.

To illustrate these capabilities, an $Al_2O_3$/Al composite is considered, being the properties of the constituents: $E = 350$ GPa and $\nu = 0.30$ for the inclusion of aluminum oxide, and $E = 70$ GPa and $\nu = 0.3$ for the aluminum matrix. The inclusion is cubic and is located at the center of the body. Three 4-node cubic beam elements are employed. Figures 7 (a) and (b) show the effective Young's modulus and Poisson ratio, respectively, for an increasing particle volume fraction. The HLE solutions (CUF-MSG) correspond to a $4^{th}$ order expansion, hereinafter HL4 model. In this case, the references correspond to those of SwiftComp [32], closed-form solutions based on ECM of $3^{rd}$ and $5^{th}$ order from Williams [12] and a mathe-

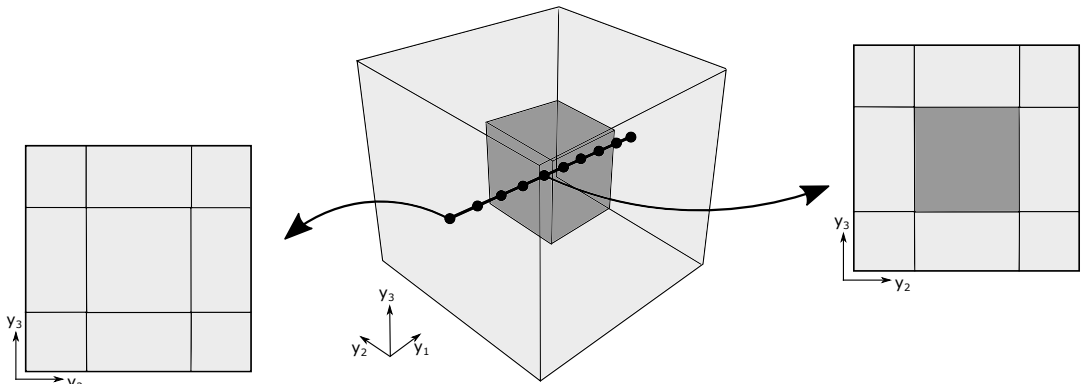


Figure 6: HLE beam model of a particle reinforced cell.

matical homogenization approach (MHT) from Banks-Sills [42]. The reference data for the graphs were extracted from [23]. Again, the HLE beam solutions are almost on top of those of the original MSG analysis, which makes use of 3D FEM elements to solve the micromechanics problem. The efficiency of the proposed model in comparison with solid modeling is shown in the next section.

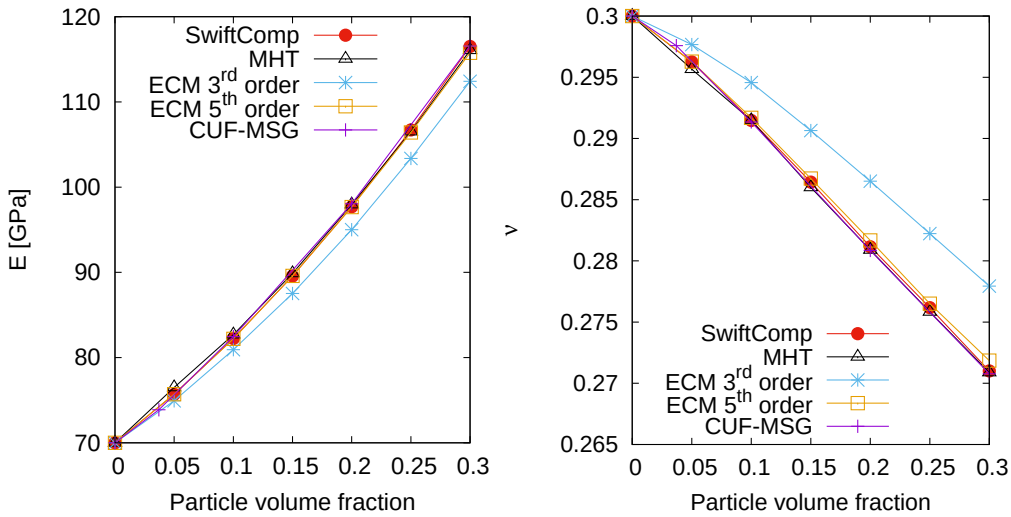


(a) Young's modulus (b) Poisson ratio

Figure 7: Effective properties of the $Al_2O_3/Al$ composite for increasing particle volume fractions.

## 5.3 Dehomogenization

The accuracy in the recovery of the local fields has a great impact in the prediction of strength and failure of the composite structure. In this section, two typical RUCs, a hexagonal pack and a cubic inclusion, are included and the performance of higher-order models on capturing high gradients in the solutions is illustrated.

### 5.3.1 Hexagonal pack

Benchmarking problems are essential in micromechanics to assess new formulations in a common framework known by the research community and to provide useful information of the advantages and drawbacks of the available methods. In this line, there are several ongoing projects that aim to set a benchmarking table for the multi-scale analysis of composites, among these the *World Wide Failure Exercise* (WWFE) [43] and the *Micromechanics Simulation Challenge* (MSC) [44]. Accordingly, the first example of this section deals with the hexagonal pack studied by Sertse *et al.* [44] in the framework of MSC. Both effective properties and local stress solutions are provided in the following and compared against those of already established micromechanical tools, including FVDAM [45, 46], GMC and HFGMC [47], DIGIMAT [48], Altair MDS [49], ESI-VPS [50], SwiftComp [32] and RVE analysis based on 3D FEA. All the details regarding the computational analysis performed with each method can be found in [44]. It is worthy to state that the RVE analysis using 3D FEA was used in the later work as a reference for all the other solutions.

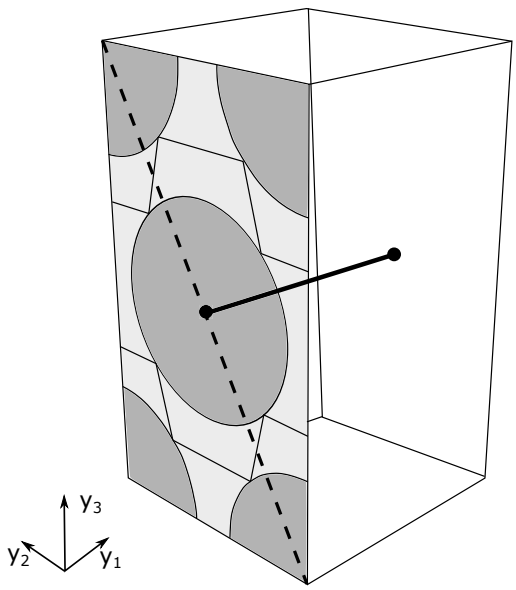


Figure 8: HLE beam model of the hexagonal pack RUC.

A carbon/epoxy composite is considered for the material properties. The fibre is modeled as transverse isotropic, with $E_1 = 276$ GPa, $E_2 = 19.5$ GPa, $G_{12} = 70$ GPa, $G_{23} = 5.74$ GPa, $\nu_{12} = 0.28$ and $\nu_{23} = 0.7$; whereas the matrix is assumed isotropic, with $E = 4.76$ GPa and $\nu = 0.37$. The fibre volume fraction is equal to 0.6. The HLE beam model for the hexagonal pack is shown in Figure 8. The cross-section consists of 15 expansion domains, including one for each fibre and ten for the matrix area. As explained before, due to the arrangement of the constituents, only one section needs to be computed. The effective properties are shown in Table 5. It should be point out that FVDAM, GMC, HFGMC and SwiftComp solutions are obtained using 2D models. HLE beam models results are in good agreement with those of the references. It is clear that the most challenging solutions are those of the transverse components, although they converge to the values of SwiftComp and 3D FEA for higher-order

models.

| Model | $E_1$ | $E_2$ | $E_3$ | $G_{12}$ | $G_{13}$ | $G_{23}$ | $\nu_{12}$ | $\nu_{13}$ | $\nu_{23}$ |
|---|---|---|---|---|---|---|---|---|---|
| | | | References [44] | | | | | | |
| FEA RVE | 167.33 | 10.67 | 10.67 | 6.38 | 6.39 | 3.33 | 0.312 | 0.312 | 0.600 |
| FVDAM | 167.30 | 10.67 | 10.67 | 6.38 | 6.39 | 3.33 | 0.310 | 0.310 | 0.600 |
| GMC | 167.40 | 10.46 | 10.08 | 5.33 | 4.45 | 3.00 | 0.312 | 0.312 | 0.612 |
| HFGMC | 167.40 | 10.71 | 10.69 | 6.58 | 6.54 | 3.36 | 0.312 | 0.312 | 0.603 |
| DIGIMAT-MF/MT | 167.52 | 10.53 | 10.53 | 6.36 | 6.36 | 3.27 | 0.312 | 0.312 | 0.605 |
| Altair MDS | 167.40 | 10.71 | 10.71 | 6.45 | 6.44 | 3.35 | 0.312 | 0.312 | 0.600 |
| ESI | 166.71 | 10.67 | 10.67 | 6.35 | 6.38 | 3.33 | 0.312 | 0.312 | 0.599 |
| SwiftComp | 167.33 | 10.67 | 10.67 | 6.38 | 6.39 | 3.33 | 0.312 | 0.312 | 0.600 |
| | | | CUF-MSG | | | | | | |
| HL2 | 167.65 | 10.84 | 10.84 | 6.56 | 6.69 | 3.40 | 0.312 | 0.312 | 0.599 |
| HL4 | 167.65 | 10.71 | 10.71 | 6.42 | 6.44 | 3.36 | 0.312 | 0.312 | 0.599 |
| HL7 | 167.65 | 10.68 | 10.68 | 6.40 | 6.41 | 3.34 | 0.312 | 0.312 | 0.600 |

Table 5: Effective properties of the hexagonal pack cell ($E_i$ and $G_{ij}$ in GPa).

A more challenging exercise is to compute the accurate local fields over the volume of the RUC. The high gradients of the strain/stress solutions demand the micromechanics model to be highly refined. For HLE beam modeling, high expansion orders are needed if one wants to capture the local solutions with an accuracy comparable to that of 3D FEA. Therefore, the HL7 model of Table 5 is used to plot the stress solutions, which are generated by applying unitary global strains. Figure 9 shows the longitudinal stress $\sigma_{11}$ generated by a unitary longitudinal strain $\varepsilon_{11}$, Figure 10 shows the shear stress $\sigma_{13}$ under shear strain $\varepsilon_{13}$, Figure 11 shows the shear stress $\sigma_{23}$ under shear strain $\varepsilon_{23}$ and Figure 12 shows the shear stress $\sigma_{12}$ under combined strains $\varepsilon_{11}$ and $\varepsilon_{13}$. The left-hand side of the aforementioned figures includes the 3D plot of the correspondent stress solutions, whereas the right-hand side plots the distribution of stresses along the diagonal of the section of the hexagonal pack (dashed line in Figure 8) for all the models considered. There is a remarkable agreement between the HLE solutions, and the 3D FEA and SwiftComp results. Even in the cases in which other micromechanics methods fail, MSG-based methods are able to provide accurately complex stress distributions and the local effects that arise in the vicinity of the interfaces.

It is obvious that HLE and SwiftComp should ideally converge to the same solutions for further refinements, since both are based in the same micromechanics approach. The focus is to show that advanced beam models can be a very efficient and convenient tool to solve composite problems, without losing the accuracy of conventional 3D FEA solutions. The computational times of each micromechanical model can be found in Table 6. All the reference times are extracted from [44]. The HLE solutions were obtained in a Windows 7 64-bit OS, Intel(R) Core(TM) i7-5500U CPU @ 2.40GHz 16.0GB RAM for all the numerical results shown in the present paper.

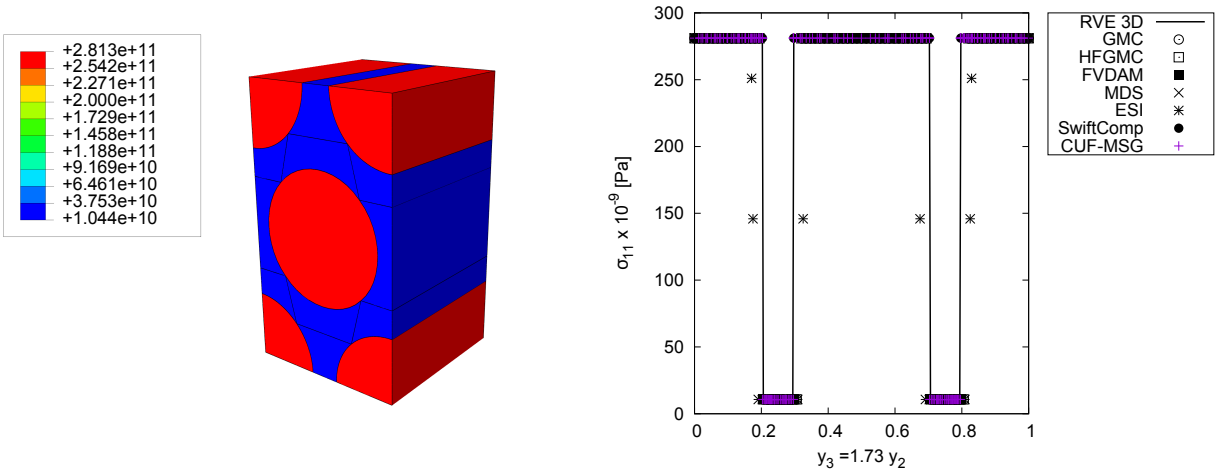


(a) $\sigma_{11}$ (b) diagonal values

Figure 9: Longitudinal stress $\sigma_{11}$ generated by a unitary longitudinal strain $\varepsilon_{11}$.

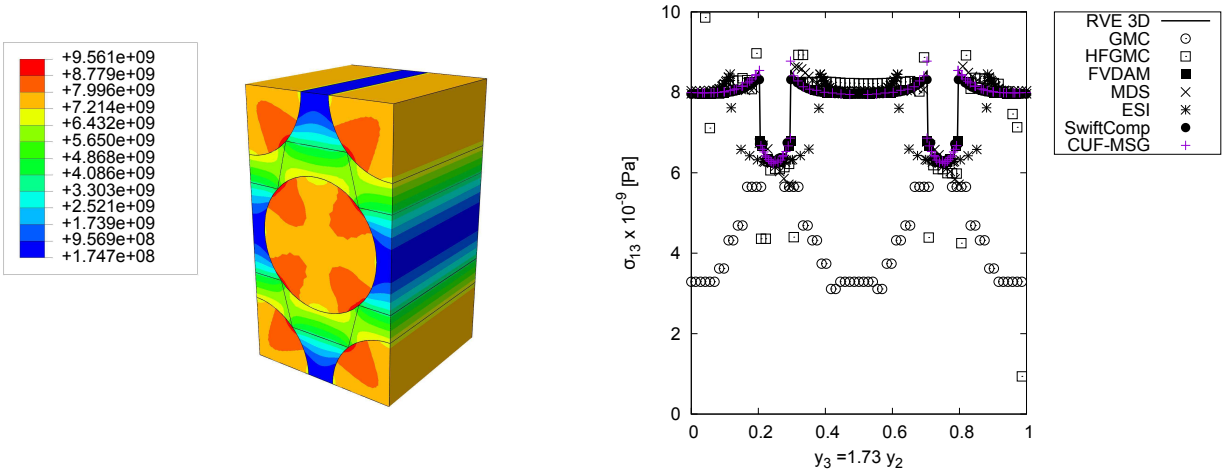


(a) $\sigma_{13}$ (b) diagonal values

Figure 10: Shear stress $\sigma_{13}$ generated by a unitary shear strain $\varepsilon_{13}$.

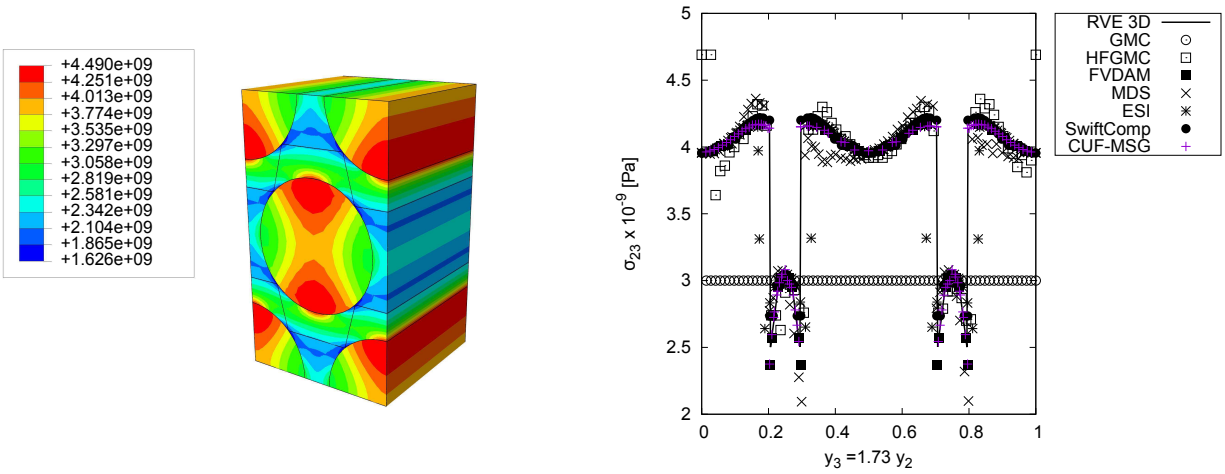


(a) $\sigma_{23}$ (b) diagonal values

Figure 11: Shear stress $\sigma_{23}$ generated by a unitary shear strain $\varepsilon_{23}$.

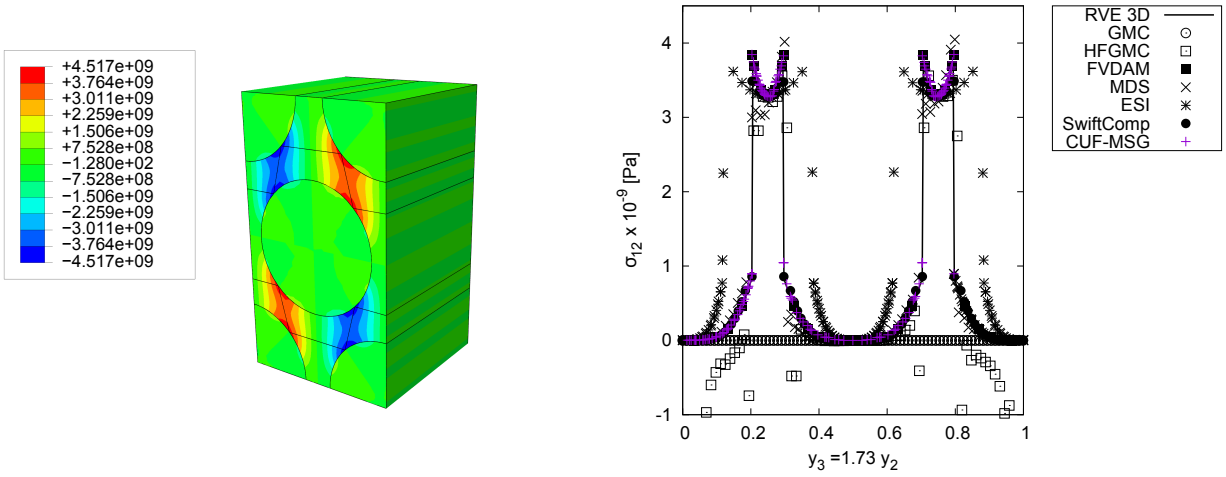


(a) $\sigma_{12}$ (b) diagonal values

Figure 12: Shear stress $\sigma_{12}$ generated by combined strains $\varepsilon_{11}$ and $\varepsilon_{13}$.

| Model | FVDAM | GMC | HFGMC | DIGIMAT | MDS | ESI | SwiftComp | HL7 | FEA |
|---|---|---|---|---|---|---|---|---|---|
| Homog. | 4 | - | - | 0.03 | 4.58 | - | 0.26 | 0.19 | - |
| Dehomog. | 0.88 | - | - | - | 5.97 | - | 0.93 | 0.73 | - |
| Total | 4.88 | 0.292 | 1.151 | - | 10.55 | 29.00 | 1.19 | 0.92 | 42.00 |

Table 6: Computing time (s) for the hexagonal pack.

### 5.3.2 Particle inclusion

The second analysis case for the local solutions corresponds to the particle reinforced composite already considered in Section 5.2. The modeling procedure and the results of the effective properties are already discussed, so now the focus is on the local stress solutions. The fibre volume fraction considered now is equal to 0.125. The cubic inclusions represent a critical test for micromechanical models due to the high stress concentrations that arise at the corners of the interfaces. The geometrical characteristics of the RUC can be exploited to reduce the computational model into a few beam elements with higher-order expansions. In order to represent accurately the local gradients along the beam axis, a total of six cubic 1D elements and nine cross-sectional domains are employed for the solutions presented hereinafter.

For this last case, SwiftComp 3D models are used as references. The longitudinal, $\sigma_{11}$, and shear, $\sigma_{13}$, stresses under the global strains $\varepsilon_{11}$ and $\varepsilon_{13}$, respectively, can be found in Figs. 13 and 14. The pictures show the 3D plots of the stresses over half of the RUC for the SwiftComp model (a) and a HL8 model (b). In Figure 13, the cell is cut through the $y_1y_3$-plane of symmetry, whereas in Figure 14 the cutting surface lays on the $y_2y_3$-plane of symmetry. One can note the differences in the modeling approaches considered and how the high-order expansions can represent the high gradients of the solutions within one expansion domain, for example at the inclusion. Finally, Figure 15 includes the distributions of stresses over the diagonal of the cell, which intersects with the vertices of the cubic inclusion.

One can notice the high stress concentrations that appear at the corners of the inclusion in

Figure 15. In this case, the solutions are obtained from three SwiftComp models of increasing mesh refinement (SC coarse, mid and refined) and two HLE models (HL4 and HL8). It is clear that in order to represent the stress solutions with fidelity, highly refined models are needed. Accordingly, the HL4 model is not enough to capture peaks in the stress solutions at the corners of the inclusion, and a HL8 model is needed to obtain a good compromise between accuracy and computational time, see Table 7.

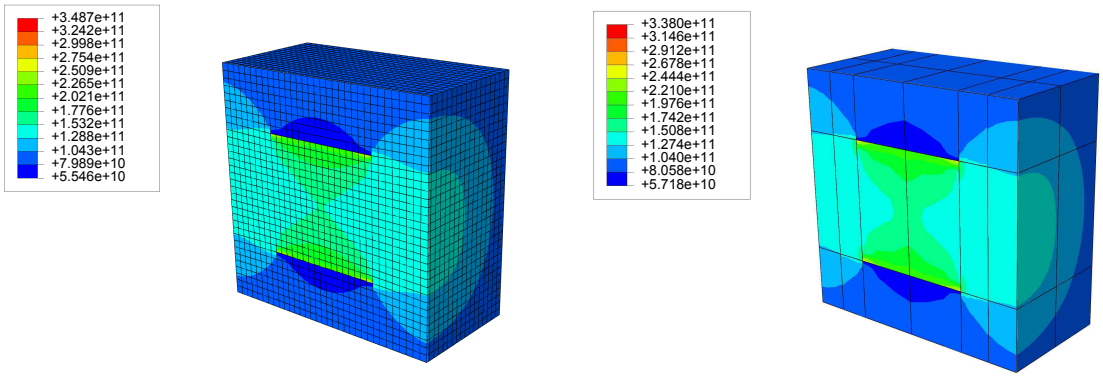


(a) SwiftComp 3D (b) HLE

Figure 13: $\sigma_{11}$ under $\varepsilon_{11}$.

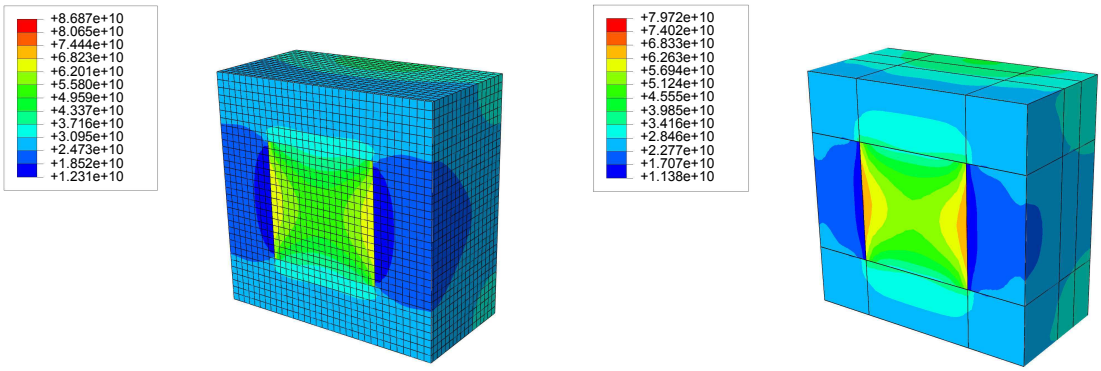


(a) SwiftComp 3D (b) HLE

Figure 14: $\sigma_{13}$ under $\varepsilon_{13}$.

| Model | SC refined | SC mid | SC coarse | HL4 | HL8 |
|---|---|---|---|---|---|
| Homogenization | 138.65 | 18.23 | 3.21 | 1.17 | 10.78 |
| Dehomogenization | 120.02 | 41.08 | 14.62 | 3.96 | 6.71 |
| Total | 258.67 | 59.31 | 17.82 | 5.13 | 17.49 |

Table 7: Computing time (s) for the particle inclusion RUC.

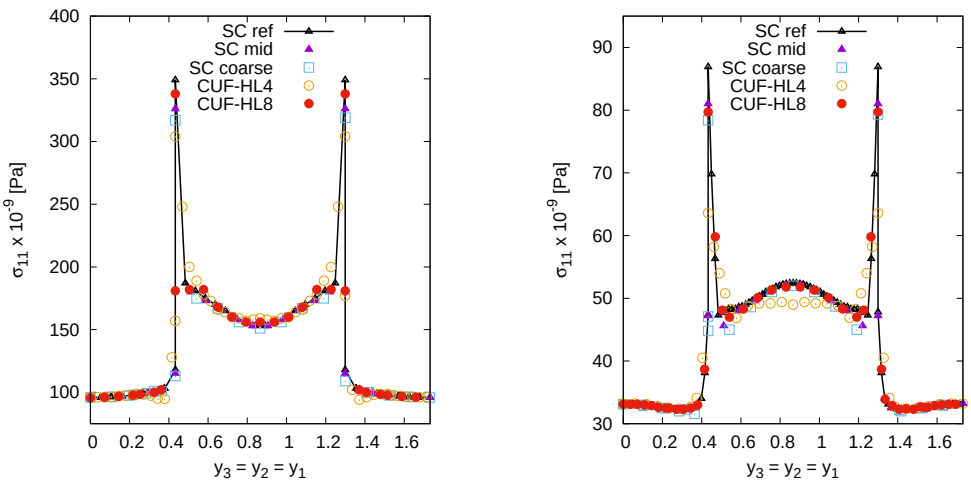


(a) $\sigma_{11}$ (b) $\sigma_{13}$

Figure 15: Stress values, $\sigma_{11}$ and $\sigma_{13}$, along the diagonal of the particle inclusion RUC.

# 6 Conclusions

This paper presents the introduction of an advanced beam modeling technique in micromechanical analysis. A computationally efficient micromechanics framework is introduced, in which the main direction of the constituents is discretized with a number of beam elements, and the remaining two directions become the cross-section of the 1D model. The characteristics of MSG are exploited to decouple the multiscale problem into local and global analysis, providing the full set of effective properties for heterogeneous anisotropic materials and arbitrary local solutions with only one single run of the code. The proposed modeling approach possesses the following unique characteristics for the RUC analysis:

- The non-isoparametric mapping technique used in HLE beam theories allows to directly insert any mathematical description of the curved edges into the model, therefore the exact geometry of the constituents is captured with a minimum number of domains.

- The discretization of the model remains fixed and the convergence of the solutions is sought by increasing the polynomial order of the beam theory, which is only a parameter of the analysis. This fact allows the user to save time in the modeling phase, avoiding the iterative refinements of the mesh that are usually required in conventional FEA analysis.

The fidelity of the solutions, both in terms of effective stiffness matrix and local fields, is proven through comparison with the MSG-based code SwiftComp, and reference solutions from the literature, including the GMC and its variants as well as RVE-FEM analysis. The high polynomial orders employed by HLE can capture even the most complex distributions, as for instance the local stress concentrations in the corners of square inclusions. The present research deals only with linear elastic cases and conventional RUCs, although its extension to more complex microstructures and nonlinear behavior remains open for future developments.

# Acknowledgments

This research work has been carried out within the project FULLCOMP (FULLy analysis, design, manufacturing, and health monitoring of COMPosite structures), funded by the European Union Horizon 2020 Research and Innovation program under the Marie Skłodowska-Curie grant agreement No. 642121. Authors would also like to acknowledge the funding received from Compagnia di San Paolo within the framework of 'Joint Projects for the Internationalization of Research'.

# References

[1] J. LLorca, C. González, J. M. Molina-Aldaregua, J. Segurado, R. Seltzer, F. Sket, M. Rodríguez, S. Sádaba, R. Muñoz, and L. P. Canal. Multiscale modeling of composite materials: a roadmap towards virtual testing. *Advanced Materials*, 23(44):5130–5147, 2011.

[2] Evan J. Pineda, Brett A. Bednarcyk, Anthony M. Waas, and Steven M. Arnold. Progressive failure of a unidirectional fiber-reinforced composite using the method of cells: Discretization objective computational results. *International Journal of Solids and Structures*, 50(9):1203 – 1216, 2013.

[3] Y. Huang, L. Xu, and S.K. Ha. Prediction of three-dimensional composite laminate response using micromechanics of failure. *Journal of Composite Materials*, 46(19-20):2431–2442, 2012.

[4] S Nemat-Nasser and M. (Muneo) Hori. *Micromechanics : overall properties of heterogeneous materials*. Amsterdam New York North-Holland, 1993.

[5] B. Hassani and E. Hinton. A review of homogenization and topology optimization ihomogenization theory for media with periodic structure. *Computers & Structures*, 69(6):707 – 717, 1998.

[6] J. Aboudi, S.M. Arnold, and B.A. Bednarcyk, editors. Butterworth-Heinemann, Oxford, 2013.

[7] R. Hill. The elastic behaviour of a crystalline aggregate. *Proceedings of the Physical Society. Section A*, 65(5):349, 1952.

[8] Z. Hashin and S. Shtrikman. A variational approach to the theory of the elastic behaviour of polycrystals. *Journal of the Mechanics and Physics of Solids*, 10(4):343 – 352, 1962.

[9] T. Mori and K. Tanaka. Average stress in matrix and average elastic energy of materials with misfitting inclusions. *Acta Metallurgica*, 21(5):571 – 574, 1973.

[10] R.M. Christensen and K.H. Lo. Solutions for effective shear properties in three phase sphere and cylinder models. *Journal of the Mechanics and Physics of Solids*, 27(4):315 – 330, 1979.

[11] T. O. Williams. A two-dimensional, higher-order, elasticity-based micromechanics model. *International Journal of Solids and Structures*, 42(34):1009 – 1038, 2005.

[12] T. O. Williams. A three-dimensional, higher-order, elasticity-based micromechanics model. *International Journal of Solids and Structures*, 42(34):971 – 1007, 2005.

[13] J. Aboudi. A continuum theory for fiber-reinforced elastic-viscoplastic composites. *International Journal of Engineering Science*, 20(5):605 – 621, 1982.

[14] M. Paley and J. Aboudi. Micromechanical analysis of composites by the generalized cells model. *Mechanics of Materials*, 14(2):127 – 139, 1992.

[15] J. Aboudi, M.J. Pindera, and S.M. Arnold. Linear thermoelastic higher-order theory for periodic multiphase materials. *Journal of Applied Mechanics*, 68(5):697 – 707, 2001.

[16] A. Bensoussan, J. Lions, and G. Papanicolaou. *Asymptotic Analysis for Periodic Structures*. North-Holland, 1978.

[17] H. Murakami and A. Toledano. A High-Order Mixture Homogenization of Bi-laminated Composites. *Journal of Applied Mechanics*, 57:388, 1990.

[18] C.T. Sun and R.S. Vaidya. Prediction of composite properties from a representative volume element. *Composites Science and Technology*, 56(2):171 – 179, 1996.

[19] W. Yu. A unified theory for constitutive modeling of composites. *Journal of Mechanics of Materials and Structures*, 11(4):379–411, 2016.

[20] V.L. Berdichevskii. On averaging of periodic systems. *Journal of Applied Mathematics and Mechanics*, 41(6):1010 – 1023, 1977.

[21] W. Yu, D.H. Hodges, and J.C. Ho. Variational asymptotic beam sectional analysis - an updated version. *International Journal of Engineering Science*, 59:40 – 64, 2012. Special Issue in honor of Victor L. Berdichevsky.

[22] W. Yu and D.H. Hodges. An asymptotic approach for thermoelastic analysis of laminated composite plates. *Journal of Engineering Mechanics*, 130(5):531–540, 2004.

[23] W. Yu and T. Tang. Variational asymptotic method for unit cell homogenization of periodically heterogeneous materials. *International Journal of Solids and Structures*, 44(11):3738 – 3755, 2007.

[24] E. Carrera. Theories and finite elements for multilayered, anisotropic, composite plates and shells. *Archives of Computational Methods in Engineering*, 9(2):87–140, 2002.

[25] E. Carrera and G. Giunta. Refined beam theories based on Carrera's unified formulation. *International Journal of Applied Mechanics*, 2(1):117–143, 2010.

[26] E. Carrera and M. Petrolo. Refined beam elements with only displacement variables and plate/shell capabilities. *Meccanica*, 47(3):537–556, 2012.

[27] E. Carrera, S. Brischetto, and A. Robaldo. Variable kinematic model for the analysis of functionally graded material plates. *AIAA Journal*, 46(1):194–203, 2008.

[28] M. Cinefra, C. Chinosi, and L. Della Croce. MITC9 shell elements based on refined theories for the analysis of isotropic cylindrical structures. *Mechanics of Advanced Materials and Structures*, 20(2):91–100, 2013.

[29] E. Carrera, M. Cinefra, E. Zappino, and M. Petrolo. *Finite Element Analysis of Structures Through Unified Formulation.* John Wiley and Sons, Ltd, 2014.

[30] E. Carrera, M. Maiarù, M. Petrolo, and G. Giunta. A refined 1D element for the structural analysis of single and multiple fiber/matrix cells. *Composite Structures*, 96:455 – 468, 2013.

[31] E. Carrera, A.G. de Miguel, and A. Pagani. Hierarchical theories of structures based on Legendre polynomial expansions with finite element applications. *International Journal of Mechanical Sciences*, (120):286–300, 2017.

[32] W. Yu and X. Liu. Swiftcomp, 2017. https://cdmhub.org/resources/scstandard.

[33] S. P. Timoshenko. On the transverse vibrations of bars of uniform cross section. *Philosophical Magazine*, 43:125–131, 1922.

[34] E. Carrera, M. Petrolo, and E. Zappino. Performance of CUF approach to analyze the structural behavior of slender bodies. *Journal of Structural Engineering*, 138(2):285–297, 2012.

[35] M. Filippi, A. Pagani, M. Petrolo, G. Colonna, and E. Carrera. Static and free vibration analysis of laminated beams by refined theory based on chebyshev polynomials. *Composite Structures*, 132:1248 – 1259, 2015.

[36] E. Carrera, M. Filippi, and E. Zappino. Laminated beam analysis by polynomial, trigonometric, exponential and zig-zag theories. *European Journal of Mechanics - A/Solids*, 41:58 – 69, 2013.

[37] B. Szabó and I. Babuska. *Finite Element Analysis.* John Wiley and Sons, Ltd, 1991.

[38] A. Pagani, A.G. de Miguel, M. Petrolo, and E. Carrera. Analysis of laminated beams via unified formulation and Legendre polynomial expansions. *Composite Structures*, pages –, 2016. In Press.

[39] E. Carrera, A. Pagani, and M. Petrolo. Classical, refined and component-wise theories for static analysis of reinforced-shell wing structures. *AIAA Journal*, 51(5):1255–1268, 2013.

[40] W.J. Gordon and C.A. Hall. Transfinite element methods: Blending-function interpolation over arbitrary curved element domains. *Numerische Mathematik*, 21(2):109–129, 1973.

[41] A. Pagani, A.G. de Miguel, and E. Carrera. Cross-sectional mapping for refned beam elements with applications to shell-like structures. 2017. Submitted.

[42] L. Banks-Sills, V. Leiderman, and D. Fang. On the effect on particle shape and orientationon elastic properties of metal matrix composites. *Composites Part B: Engineering*, 28B:465–481, 1997.

[43] M.J. Hinton, A.S. Kaddour, and P.D. Soden. *Failure Criteria in Fibre-Reinforced-Polymer Composites. The World-Wide Failure Exercise.* Oxford: Elsevier, 2000.

[44] H. M Sertse, J. Goodsell, A. J. Ritchey, R. B. Pipes, and W. Yu. Challenge problems for the benchmarking of micromechanics analysis: Level I initial results. *Journal of Composite Materials*, 0(0):1–20, 2017.

[45] M. A.A. Cavalcante, M-J. Pindera, and H. Khatam. Finite-volume micromechanics of periodic materials: Past, present and future. *Composites Part B: Engineering*, 43(6):2521 – 2543, 2012.

[46] M. A.A. Cavalcante, M-J. Pindera, and H. Khatam. Generalized FVDAM theory for periodic materials undergoing finite deformationspart I: Framework. *Journal of Applied Mechanics*, 81(2):021005, 2013.

[47] B.A. Bednarcyk and S.M. Arnold. Mac/gmc 4.0 user's manual,volume 2: keywords manual, tm 2002-212077. *Journal of Constructional Steel Research*, 2, 2002.

[48] *DIGIMAT user's manual (Release 5.1.2, 2014).* e-Xstream MSC Software Company.

[49] J. Fish and Q. Yu. Computational mechanics of fatigue and life predictions for composite materials and structures. *Computer Methods in Applied Mechanics and Engineering*, 191(43):4827 – 4849, 2002.

[50] ESI Group. *Virtual Performance Solution. Solver Notes Manual.* 2013.

# A Fundamental nuclei arrays

The explicit expressions of the nine components of the $\boldsymbol{E}^{\tau sij}$ fundamental nucleus, for the case of orthotropic constituents, are:

$$
\begin{aligned}
E_{22}^{\tau sij} &= C_{22} \int_l N_i\, N_j\, \mathrm{d}y_1\, S_{\tau,x\,s,x} \,+\, C_{44} \int_l N_i\, N_j\, \mathrm{d}y_1\, S_{\tau,z\,s,z} \,+\, C_{66} \int_l N_{i,y1}\, N_{j,y1}\, \mathrm{d}y_1\, S_{\tau s} \\
E_{21}^{\tau sij} &= C_{21} \int_l N_i\, N_{j,y1}\, \mathrm{d}y_1\, S_{\tau,x\,s} \,+\, C_{66} \int_l N_{i,y1}\, N_j\, \mathrm{d}y_1\, S_{\tau s,x} \\
E_{23}^{\tau sij} &= C_{32} \int_l N_i\, N_j\, \mathrm{d}y_1\, S_{\tau,x\,s,z} \,+\, C_{44} \int_l N_i\, N_j\, \mathrm{d}y_1\, S_{\tau,z\,s,x} \\
E_{12}^{\tau sij} &= C_{21} \int_l N_{i,y1}\, N_j\, \mathrm{d}y_1\, S_{\tau s,x} \,+\, C_{66} \int_l N_i\, N_{j,y1}\, \mathrm{d}y_1\, S_{\tau,x\,s} \\
E_{11}^{\tau sij} &= C_{11} \int_l N_{i,y1}\, N_{j,y1}\, \mathrm{d}y_1\, S_{\tau s} \,+\, C_{55} \int_l N_i\, N_j\, \mathrm{d}y_1\, S_{\tau,z\,s,z} \,+\, C_{66} \int_l N_i\, N_j\, \mathrm{d}y_1\, S_{\tau,x\,s,x} \\
E_{13}^{\tau sij} &= C_{31} \int_l N_{i,y1}\, N_j\, \mathrm{d}y_1\, S_{\tau s,z} \,+\, C_{55} \int_l N_i\, N_{j,y1}\, \mathrm{d}y_1\, S_{\tau,z\,s} \\
E_{32}^{\tau sij} &= C_{32} \int_l N_i\, N_j\, \mathrm{d}y_1\, S_{\tau,z\,s,x} \,+\, C_{44} \int_l N_i\, N_j\, \mathrm{d}y_1\, S_{\tau,x\,s,z} \\
E_{31}^{\tau sij} &= C_{31} \int_l N_i\, N_{j,y1}\, \mathrm{d}y_1\, S_{\tau,z\,s} \,+\, C_{55} \int_l N_{i,y1}\, N_j\, \mathrm{d}y_1\, S_{\tau s,z} \\
E_{33}^{\tau sij} &= C_{33} \int_l N_i\, N_j\, \mathrm{d}y_1\, S_{\tau,z\,s,z} \,+\, C_{44} \int_l N_i\, N_j\, \mathrm{d}y_1\, S_{\tau,x\,s,x} \,+\, C_{55} \int_l N_{i,y1}\, N_{j,y1}\, \mathrm{d}y_1\, S_{\tau s}
\end{aligned}
\tag{37}
$$

where the $S$ terms correspond to the integrals of the transverse expansions over the cross-section surface, defined as

$$
\begin{aligned}
S_{\tau,x s,x} &= \int_\Omega F_{\tau,x} F_{s,x}\, d\Omega, \quad S_{\tau,z s,z} = \int_\Omega F_{\tau,z} F_{s,z}\, d\Omega, \quad S_{\tau s} = \int_\Omega F_\tau F_s\, d\Omega, \\
S_{\tau,x s,z} &= \int_\Omega F_{\tau,x} F_{s,z}\, d\Omega, \quad S_{\tau,z s,x} = \int_\Omega F_{\tau,z} F_{s,x}\, d\Omega, \quad S_{\tau,x s} = \int_\Omega F_{\tau,x} F_s\, d\Omega, \\
S_{\tau s,x} &= \int_\Omega F_\tau F_{s,x}\, d\Omega, \qquad S_{\tau,z s} = \int_\Omega F_{\tau,z} F_s\, d\Omega, \qquad S_{\tau s,z} = \int_\Omega F_\tau F_{s,z}\, d\Omega,
\end{aligned}
\tag{38}
$$

On the other hand, the eighteen components of the $3 \times 6$ $\boldsymbol{D}_{h\varepsilon}^{\tau i}$ fundamental nucleus read:

$$
\begin{aligned}
D_{h\varepsilon 11}^{\tau i} &= C_{11} \int_l N_{i,y1} \mathrm{d}y_1 \int_\Omega F_\tau \, d\Omega & D_{h\varepsilon 12}^{\tau i} &= C_{12} \int_l N_{i,y1} \mathrm{d}y_1 \int_\Omega F_\tau \, d\Omega \\
D_{h\varepsilon 13}^{\tau i} &= C_{13} \int_l N_{i,y1} \mathrm{d}y_1 \int_\Omega F_\tau \, d\Omega & D_{h\varepsilon 14}^{\tau i} &= 0 \\
D_{h\varepsilon 15}^{\tau i} &= C_{55} \int_l N_i \mathrm{d}y_1 \int_\Omega F_{\tau,z} \, d\Omega & D_{h\varepsilon 16}^{\tau i} &= C_{66} \int_l N_i \mathrm{d}y_1 \int_\Omega F_{\tau,x} \, d\Omega \\
D_{h\varepsilon 21}^{\tau i} &= C_{12} \int_l N_i \mathrm{d}y_1 \int_\Omega F_{\tau,x} \, d\Omega & D_{h\varepsilon 22}^{\tau i} &= C_{22} \int_l N_i \mathrm{d}y_1 \int_\Omega F_{\tau,x} \, d\Omega \\
D_{h\varepsilon 23}^{\tau i} &= C_{23} \int_l N_i \mathrm{d}y_1 \int_\Omega F_{\tau,x} \, d\Omega & D_{h\varepsilon 24}^{\tau i} &= C_{44} \int_l N_i \mathrm{d}y_1 \int_\Omega F_{\tau,z} \, d\Omega \\
D_{h\varepsilon 25}^{\tau i} &= 0 & D_{h\varepsilon 26}^{\tau i} &= C_{66} \int_l N_{i,y1} \mathrm{d}y_1 \int_\Omega F_\tau \, d\Omega \\
D_{h\varepsilon 31}^{\tau i} &= C_{13} \int_l N_i \mathrm{d}y_1 \int_\Omega F_{\tau,z} \, d\Omega & D_{h\varepsilon 32}^{\tau i} &= C_{23} \int_l N_i \mathrm{d}y_1 \int_\Omega F_{\tau,z} \, d\Omega \\
D_{h\varepsilon 33}^{\tau i} &= C_{33} \int_l N_i \mathrm{d}y_1 \int_\Omega F_{\tau,z} \, d\Omega & D_{h\varepsilon 34}^{\tau i} &= C_{44} \int_l N_i \mathrm{d}y_1 \int_\Omega F_{\tau,x} \, d\Omega \\
D_{h\varepsilon 25}^{\tau i} &= C_{55} \int_l N_{i,y1} \mathrm{d}y_1 \int_\Omega F_\tau \, d\Omega & D_{h\varepsilon 26}^{\tau i} &= 0
\end{aligned}
\tag{39}
$$